NANO LETTERS

pubs.acs.org/NanoLett Letter

Controlling Intracellular Enzymatic Self-Assembly of Peptide by Host–Guest Complexation for Programming Cancer Cell Death

Xuejiao Yang,[#] Bihan Wu,[#] Jiong Zhou, Honglei Lu, Hongyue Zhang, Feihe Huang, and Huaimin Wang*

Cite This: *Nano Lett.* 2022, 22, 7588–7596 Read Online

ACCESS | Metrics & More | Article Recommendations | Supporting Information

ABSTRACT: Controlling the enzymatic reaction of macromolecules in living systems plays an essential role in determining the biological functions, which remains challenging in the synthetic system. This work shows that host–guest complexation could be an efficient strategy to tune the enzymatic self-assembly of the peptide. The formed host–guest complexation prevents the enzymatic kinetics of peptide assemblies on the cell surface and promotes cellular uptake of assemblies. For uptake inside cells, the host–guest complex undergoes dissociation in the acidic lysosome, and the released peptide further self-assembles inside the mitochondria. Accumulating assemblies at mitochondria induce the ferroptosis of cancer cells, resulting in cancer cell death *in vitro* and the tumor-bearing mice model. As the first example of using host–guest complexation to modulate the kinetics of enzymatic self-assembly, this work provides a general method to control enzymatic self-assembly in living cells for selective programming cancer cell death.

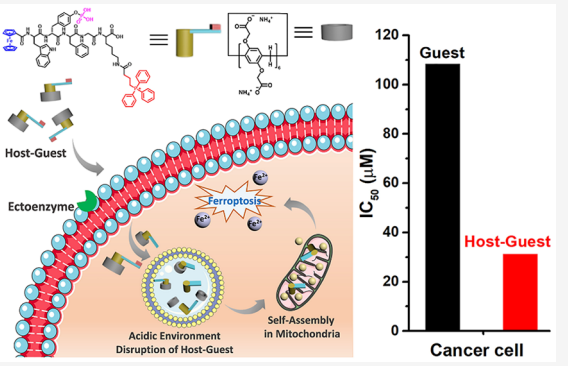

KEYWORDS: *peptide, host–guest complexation, enzymatic instructed self-assembly, mitochondria, cancer therapy*

Self-assembly[1,2] can be employed to create higher-order assemblies in a specific location with emergent biological properties and functions that cannot be achieved by monomeric molecules. Remarkably, enzyme instructed self-assembly, mimicking the most biological processes (e.g., actin dynamics, signalosomes, and granules[3]) in the living systems, is the most efficient strategy to control the kinetics of molecular assemblies. Inspired by the natural enzymatic processes and functional assemblies in living cells, the recent emergent strategy for cancer therapy, which differs from conventional approaches (chemotherapy, immunotherapy, and targeted therapy), is to generate chemical assemblies of small molecules in situ of cancer cells.[4−17] A recent remarkable example of such a strategy is to use enzyme-induced self-assembly (EISA) to control cell behavior around or inside cells by an over-expressing enzyme.[18−22] More importantly, the formation rate of enzymatic assemblies is the key factor for their cell targeting ability and final bioactivity. However, regulating EISA kinetics with organelle targeting in a simple way for cancer therapy remains challenging. Thus, developing a general strategy to control the kinetics of EISA of small molecules in living cells would be highly urgent.[23,24]

Herein, we report using the host–guest complexation,[25−28] which has been extensively explored in sensing, regulating protein functions, and drug delivery, to modulate the kinetics of EISA assemblies' formation in cancer cells with mitochondria targeting and inducing cancer cell death selectively. To achieve the approach, we designed enzyme responsive peptide with the N-terminal modification of the ferrocenyl group (Figure 1A), which can interact with pillar[6]arene (**WP6**) to form a pH-sensitive host–guest complex (Figure 1B). The formed complex prevents the enzymatic reaction on the cell surface and promotes cellular uptake of peptides. Assemblies of the host–guest complex can escape from lysosomes and further self-assemble inside the targeted organelle (mitochondria) due to increased local concentration. Accumulating assemblies at mitochondria induce the ferroptosis of cancer cells, resulting in cancer cell death selectively (Figure 1C). This work illustrates a general strategy to kinetically control enzymatic assemblies in living cells for selective programming cancer cell death, which offers a new avenue for targeted cancer therapy through *in vivo* self-assembly of organic compounds.

Based on the above concept, we designed the peptide Fc-^{D}Wp^{D}Y^{D}FG^{D}K-TPP (**Fc-TPP1**), which contains the self-assembling motif: tryptophan (W)-tyrosine (Y)-phenylalanine (F) that favors self-assembly through inherent hydrogen

Received: July 3, 2022
Revised: July 26, 2022
Published: August 4, 2022

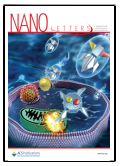

https://doi.org/10.1021/acs.nanolett.2c02612
Nano Lett. 2022, 22, 7588–7596

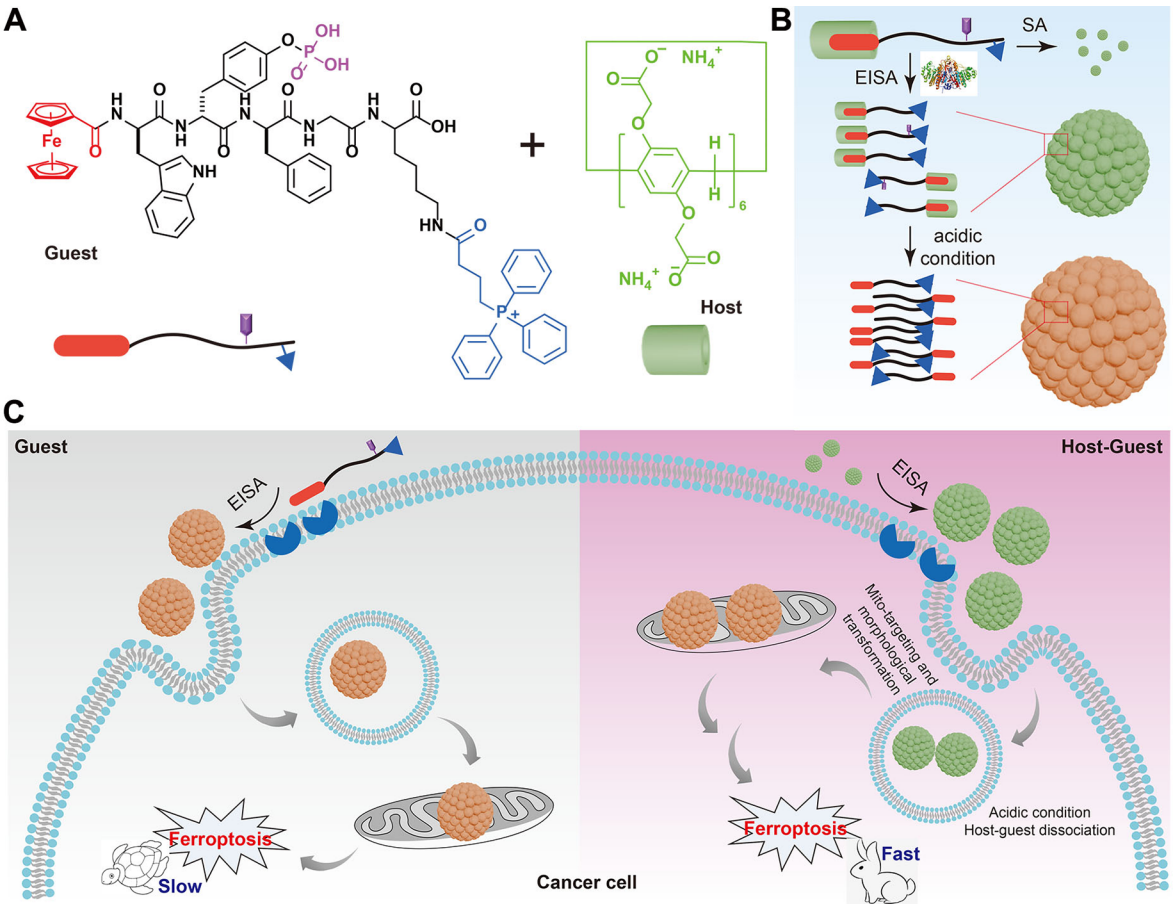

Figure 1. (A) Chemical structures of Fc-^{D}Wp^{D}Y^{D}FG^{D}K-TPP (**Fc-TPP1**) and pillar[6]arene **WP6**. (B) Schematic illustration of (i) assemblies formed from the host−guest complexes between **Fc-TPP1** and **WP6** molecules, (ii) nanostructures formed from enzyme induced self-assembly of the **Fc-TPP1**/**WP6** host−guest complexes, (iii) acid-induced dissociation of host−guest complexation and reassembly. (C) In cancer cells, the formation of the host−guest complex increases the cellular uptake of peptides. The acidic environment in the lysosome dissociates host−guest complexation, and the nanostructures are reassembled by **Fc-TPP1** at mitochondria, resulting in cancer cell death.

bonding and $\pi-\pi$ interaction.[29] The introduction of phosphotyrosine is for cancer cell-selective targeting, which could respond to the overexpressed alkali phosphatase (ALP) on some cell membranes.[30−32] The triphenylphosphine (TPP) group at the side chain of lysine is used to target the mitochondria matrix of cells.[33] The ferrocenyl group (Fc) serves as a guest motif for a synthetic macrocyclic host[34] of pillar[6]arene (**WP6**) to form a host−guest complex. Such a design allows us to use the host−guest complexation between the pillar[6]arene host and the Fc guest to control the enzymatic self-assembly of **Fc-TPP1**. Since the host−guest complex of **Fc-TPP1** and **WP6** has the pH-responsive property,[35] the guest molecules could easily escape from the lysosome and are transported into the mitochondria matrix of cancer cells. After synthesizing **Fc-TPP1** using the standard solid phase peptide synthesis and solution coupling (Figure S1), we used HPLC to purify the compounds and verified them by LC-MS and NMR (Figures S2−S4).

Isothermal titration calorimeter (ITC) experiments show that titrating **Fc-TPP1** into **WP6** is an exothermic process with a binding constant (K_D) of 39.9 μM and a binding number of 1.23, suggesting Fc capped peptide does not influence the host−guest interaction of Fc and **WP6** (Figures S5, S6A). The continuous variation method (Job's plot) using UV−vis spectroscopy further confirms the 1:1 binding stoichiometry between **Fc-TPP1** and **WP6** (Figures S6B, S7), agreeing with the previous report.[35] HPLC results (Figures S8, S9) reveal that the hydrolysis rate of **Fc-TPP1** is faster than the host−guest complex in the presence of ALP. The $t_{1/2}$ of **Fc-TPP1** and the host−guest complex is 25.6 and 51.8 min (Figure S6C), respectively, indicating the formation of host−guest interaction prevents the enzymatic hydrolysis of the guest molecule.

TEM results indicate that **WP6** (Figure S10) forms amorphous nanostructures (50 μM) in aqueous solution (pH 7.4), without the Tyndall effect. **Fc-TPP1** self-assembles into nanoaggregates consisting of small particles in the absence of ALP (Figures S6D, S11A). Mixing **Fc-TPP1** with **WP6** results in the morphology transforming into aggregates with a smaller size (Figures S6D, S11B−D), but without the Tyndall effect (Figure S12). After adding ALP, the solution of **Fc-TPP1** with **WP6** exhibits a clear Tyndall effect (Figure S6D), indicating the existence of abundant assemblies. Moreover, we observed morphology transformation from small aggregated nanoparticles into nanospheres with diameters of several hundred nanometers (Figure S11E−H). Specifically, **Fc-TPP1** transforms into uniform nanospheres with an average diameter of 150 nm. The host−guest complex at a molar ratio of 1:1 (**Fc-TPP1**:**WP6**) forms nanospheres with a diameter of 200 nm, consisting of the results of dynamic light scattering (DLS, Figure S13). Interestingly, the diameter of nanospheres formed by the host−guest complex decreases with the increase of **WP6**

https://doi.org/10.1021/acs.nanolett.2c02612
Nano Lett. 2022, 22, 7588−7596

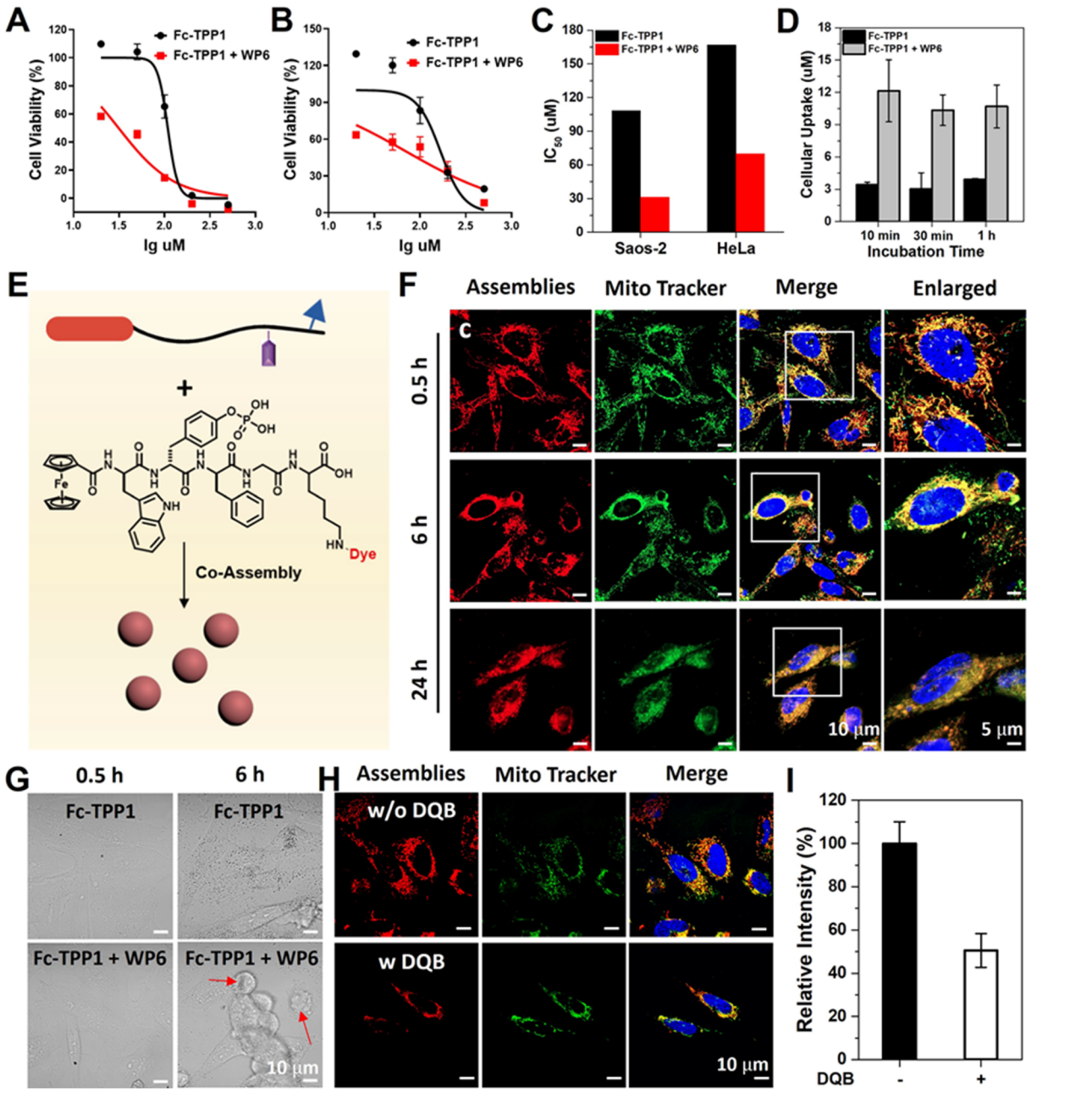

Figure 2. Cytotoxicity (24 h) of **Fc-TPP1** and the **Fc-TPP1/WP6** host–guest complex against (A) Saos-2 cells and (B) HeLa cells. (C) Summary of the IC_{50} values of **Fc-TPP1** and the host–guest complex against Saos-2 and HeLa cells for 24 h. (D) LC-MS analysis of the concentration of **Fc-TPP1** in **Fc-TPP1** or **Fc-TPP1/WP6** treated Saos-2 cells for 10 min, 30 min, and 1 h, respectively. (E) Illustration of coassembly of the fluorophore-labeled peptide with **Fc-TPP1**. (F) CLSM images of Saos-2 cells incubated with the host–guest complex for 0.5, 6, and 24 h, respectively. (G) DIC images of Saos-2 cells incubated with **Fc-TPP1** and the host–guest complex for 0.5 and 6 h, respectively. (H) CLSM images and (I) the corresponding fluorescence intensity of Saos-2 cells incubated with the host–guest complex in the absence and presence of DQB (20 μM) for 2 h.

after the addition of ALP, indicating the optimized ratio for **Fc-TPP1** and **WP6** is 1:1. These results imply that we can use host–guest interaction to tune the kinetics of enzymatic self-assembly of peptides, which has not been reported previously. Under acidic conditions (pH 5.0), the formed nanospheres of host–guest complexation disappeared, as evidenced by a dramatic decrease in scattering intensity and TEM results (Figure S14). Furthermore, the nanospheres and Tyndall effect could be recovered (Figure S15) after adjusting the pH to a neutral condition (pH 7.4), suggesting the pH-responsive property and reversibility of host–guest complexation.

To investigate whether controlling enzymatic kinetics of assemblies by the host–guest interaction could be applied in living cells. We choose Saos-2 and HeLa cell lines as the cancer cell models because of overexpressing ALP on and inside these cell lines. We also used a normal cell line HS-5 as a control group. The cytotoxicity experiment indicates that **WP6** shows low cytotoxicity against Saos-2, HeLa, and HS-5 cells, suggesting the good biocompatibility of **WP6** (Figure S16). **Fc-TPP1** exhibits cytotoxicity against Saos-2 cells and HeLa cells in a dose-dependent manner while innocuous to HS-5 cells (Figures 2A, B, and S17B). The IC_{50} of **Fc-TPP1** is 108.4

https://doi.org/10.1021/acs.nanolett.2c02612
Nano Lett. 2022, 22, 7588–7596

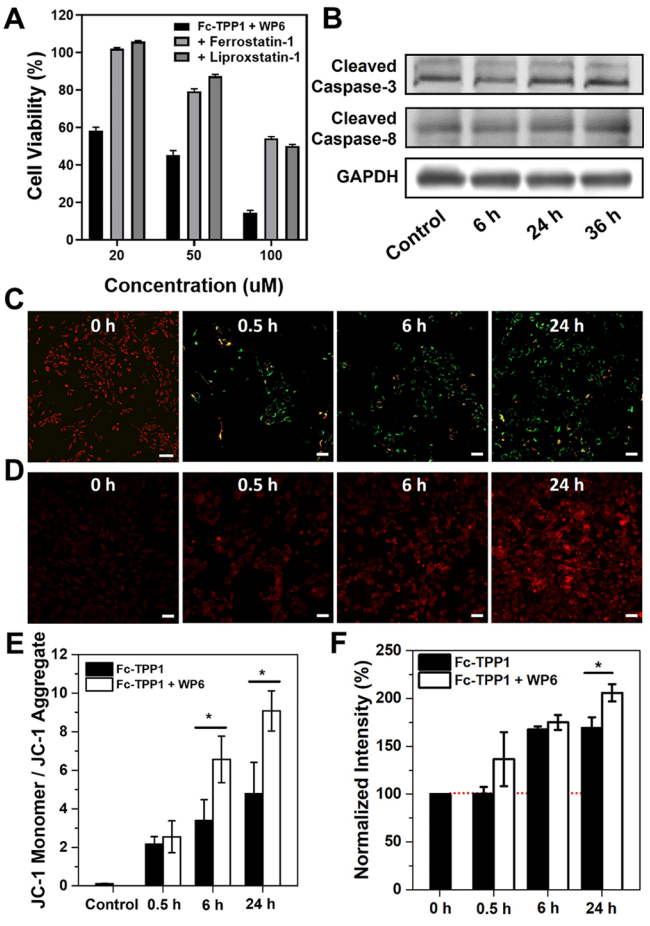

Figure 3. (A) Cytotoxicity (24 h) of the **Fc-TPP1/WP6** host–guest complex without or with the addition of Ferrostatin-1 and Liproxstatin-1 against Saos-2 cells, respectively. (B) Time-dependent Western blot analysis of cleaved caspase-3 and caspase-8 of Saos-2 cells treated with **Fc-TPP1/WP6** for 6, 24, and 36 h, respectively. CLSM images of (C) JC-1 and (D) DHE staining in Saos-2 that treated with the host–guest complex (50 μM) for 0.5, 6, and 24 h, respectively. (E) Quantitative analysis of JC-1 monomer (red fluorescence)/JC-1 aggregates (green fluorescence) ratios, which was calculated from (C). (F) Quantitative analysis of fluorescent intensity in (D). The concentrations of **Fc-TPP1** and **WP6** are 50 μM. Scale bars in (C) and (D) are 100 μm and 50 μm, respectively. Each experiment is repeated 3 individual times.

μM against Saos-2 cells, which is about 3.5-fold higher than the IC_{50} of the host–guest complex (31.2 μM). The IC_{50} of **Fc-TPP1** and the host–guest complex against HeLa cells follow the same order: about 167.1 μM and 70.2 μM, respectively (Figure 2C). In addition, the IC_{50} of **Fc-TPP1** and host–guest complex against HS-5 cells is higher than 300 μM (Figure S17C, D), suggesting the selectivity of the host–guest complex toward cancer cells. These results suggest that the host–guest interaction can modulate the enzymatic kinetics in living cells and control the bioactivity of intracellular assemblies through EISA in living cancer cells.

We next quantified the relevant concentration of peptides in Saos-2 cells. LC-MS analysis indicated that the concentration of **Fc-TPP1** in host–guest complexation treated cells reaches 10.2 μM after 1 h of incubation, which is about 3 times higher than that of **Fc-TPP1** (3.5 μM) treated cells (Figures 2D, S18). The results also showed that the enzymatic hydrolysis rate of **Fc-TPP1** in host–guest complexation treated cells is 35.1%, while it is only 5.2% for **Fc-TPP1** treated cells (Figure S18D, F). These results indicated that the host–guest complexation could promote the cellular uptake of **Fc-TPP1** precursors. After disrupting the host–guest complex inside acidic lysosomes, the fast enzymatic hydrolysis and self-assembly would proceed inside cells.

To directly visualize the formation of assemblies inside cells, we used a fluorescent molecule Fc-^{D}Wp^{D}Y^{D}FG^{D}K-Cy5.5 (**Fc-Cy5.5**, Figures S19, S20), which can coassemble with **Fc-TPP1** to form hybrid nanospheres (Figures 2E, S21). We first investigated the modes of endocytosis involved in host–guest complex treated cells. After incubating Saos-2 cells with the host–guest complex at 4 °C for 2 h, we hardly observed any red fluorescence associated with cell membranes or inside cells (Figures S22, S23), indicating that uptake of the host–guest complex by cells is energy-dependent. We next incubated Saos-2 cells with different endocytotic inhibitors. The results showed that adding chlorpromazine (an inhibitor of a clathrin-mediated endocytosis inhibitor) and Filipin III (an inhibitor of caveolae-mediated endocytosis) could reduce the uptake of the host–guest complex by about 21.4% and 14.3%, respectively. The results indicated that the host–guest complex mainly undergoes clathrin-mediated endocytosis and caveolae-mediated endocytosis, ensuring the accumulation of assemblies at mitochondria after cellular uptake. Moreover, to demonstrate the host–guest complex in acidic endosomes, we incubated Saos-2 cells with Bafilomycin A1, an inhibitor of lysosomal acidification by preventing the passage of protons into the lysosomal lumen. The results showed that the addition of Bafilomycin A1 could reduce the uptake of the host–guest complex significantly (Figures S24, S25), indicating that the uptake of the host–guest complex is involved in the lysosome-related pathway.

Time-dependent CLSM experiments showed that the red fluorescence from assemblies formed by the host–guest complex could colocalize with the green fluorescence from the mito-tracker (Figure 2F) after incubating the host–guest complex for 0.5 h with Saos-2 cells, indicating the nanostructures could accumulate into the mitochondria rapidly. With the increase of incubating time to 6 h, CLSM indicates the fragmentation of mitochondria[36] and the cells become unhealthy. After 24 h of incubation, the cells shrunk, and assemblies that exhibit red fluorescence are still located at the mitochondria. For **Fc-TPP1** treated Saos-2 cells (Figure S26), after incubating for 0.5 and 6 h, the red fluorescence formed by **Fc-TPP1** could overlap with mito-tracker, and the mitochondria of cells exhibit tubular structures, which is similar to the cells without any treatment. In contrast, the mitochondria of cells treated with host–guest complex exhibit severe damage than **Fc-TPP1** treated cells. As shown in Figure 2G, DIC images show that the cells treated with the host–guest complex exhibit apoptotic morphology compared with those treated with **Fc-TPP1** for 6 h at the same concentration (Figure 2G).[37] These results indicate that the host–guest complex can control the formation of enzymatic assemblies of peptides in living cancer cells and increase their retention time on mitochondria, resulting in fast cancer cell death with higher bioactivity. Co-incubating a tissue-nonspecific ALP inhibitor (DQB) with the host–guest complex significantly decreased the red fluorescence from assemblies in the mitochondria (Figures 2H and 2I), indicating the role of the enzyme in the mitochondria-targeted self-assembly process.

https://doi.org/10.1021/acs.nanolett.2c02612
Nano Lett. 2022, 22, 7588–7596

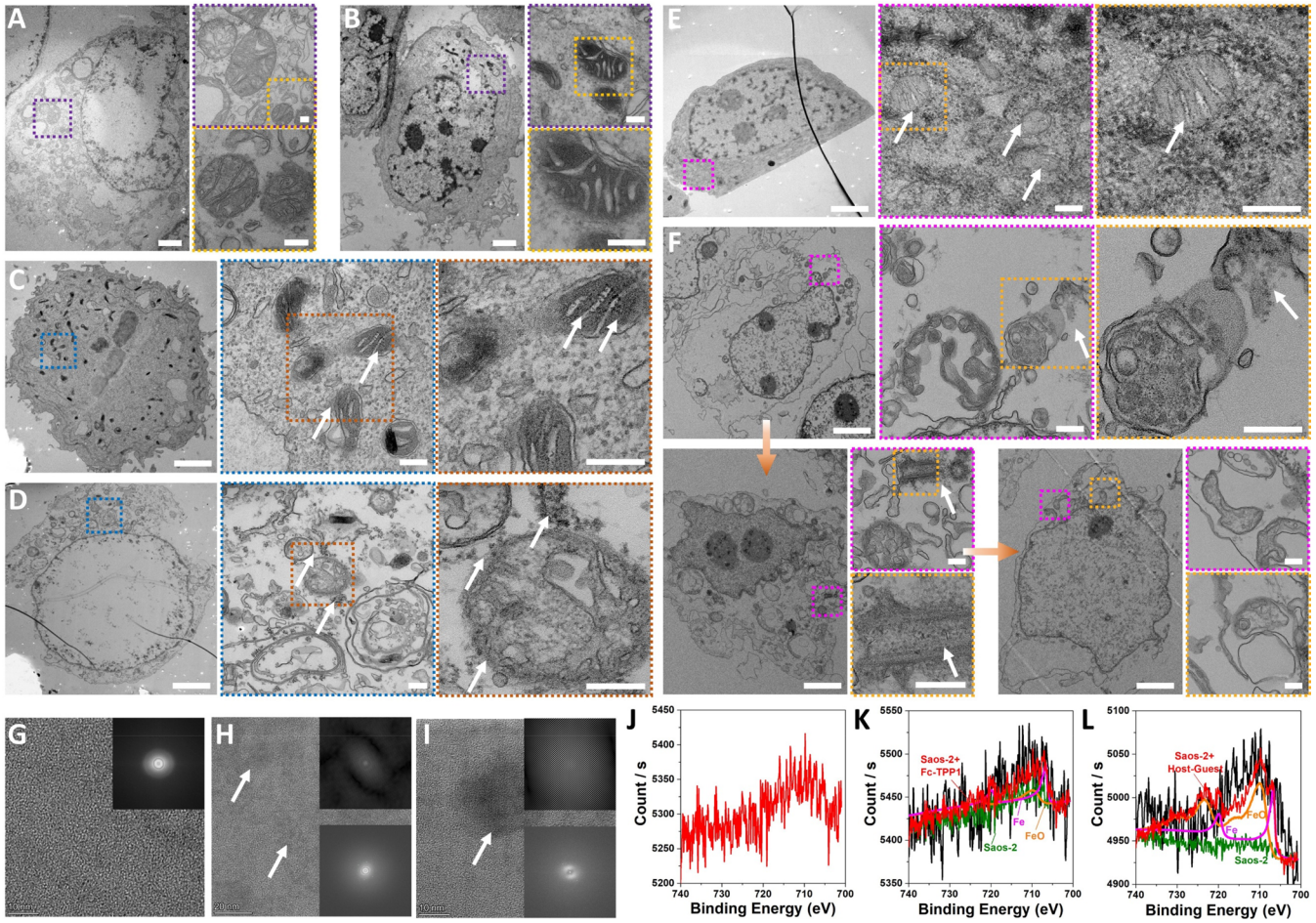

Figure 4. Bio-TEM images: (A) Saos-2 cells; (B) treated with **WP6** for 24 h; (C) treated with **Fc-TPP1** for 0.5 h; (D) treated with **Fc-TPP1** for 24 h; (E) treated with the **Fc-TPP1/WP6** host−guest complex for 0.5 h; (F) treated with the **Fc-TPP1/WP6** host−guest complex for 24 h. High-magnification TEM images, corresponding FFT pattern, and XPS spectra of Saos-2 cells: (G, J) without treatment; (H, K) treated with **Fc-TPP1**; (I, L) treated with the host−guest complex for 24 h. Scale bars of whole cells and enlarged images in (A-F) are 2 μm and 200 nm, respectively. The white arrows in (C−F) and (H, I) indicate the black dots and lattice fringes, respectively.

To explore the modality of cell death induced by the host−guest complex, we first coincubate two inhibitors of ferroptosis (Ferrostatin-1 and Liproxstatin-1)[38,39] with the host−guest complex in the culture of Saos-2 cells. The results indicate that both inhibitors could rescue the cells from 14% to 54% and 50% (100 μM, Figure 3A), respectively. Western blot experiments also show the increased apoptosis induced by the host−guest complex as time evolves (Figures 3B, S27). These results indicate that the host−guest complex induces cell death involving ferroptosis and apoptosis.

We next used the JC-1 kit to study the variation of mitochondrial membrane potential. The cells without any treatment exhibit red fluorescence (Figure 3C). The intensity of red fluorescence of Saos-2 cells treated with **Fc-TPP1** or host−guest complex decreases significantly, while the green fluorescence increases (Figures 3C, E, and S28) with the increase of incubation time. These results indicate that the mitochondrial membrane potential decreased after the treatment of **Fc-TPP1** and the host−guest complex. Quantitative analysis indicates that the JC-1 monomer/aggregate ratio increased with the extension of incubation time. At the same time point, the host−guest complex treated Saos-2 cells showed a higher ratio of JC-1 monomer/aggregate than the cells treated with **Fc-TPP1**, indicating the severe damage of Saos-2 cells that incubated with the host−guest complex, consisting of the cell viability experiments and CLSM results (Figure 2F and G).

We then detected the generation of ROS in cells using Dihydroethidium (DHE) probe[40] because the generation of ROS is an indicator of ferroptosis.[41−43] The results show that the red fluorescence in Saos-2 cells increased gradually after coincubating with **Fc-TPP1** or the host−guest complex (Figures 3D, S29). The Saos-2 cells without any treatment only show very weak red fluorescence. The fluorescent intensity of the cells treated with the host−guest complex is stronger than those treated with **Fc-TPP1**, as evidenced by the quantitative analysis (Figure 3F). Flow cytometry (FCM) analysis also indicates that the fluorescent intensity of DHE in Saos-2 cells increased gradually with the extension of incubation time when treated with **Fc-TPP1** and the host−guest complex (Figure S30).

Bio-TEM experiments indicate that the cells without treatment or treated with **WP6** (24 h) are integral, and the mitochondria in these cells are healthy (Figure 4A, 4B). In contrast, the cells treated with **Fc-TPP1** after 0.5 h show many black dots at the mitochondria (Figure 4C). Considering the apparent contrast of nanostructures, we speculate that the self-assembly of **Fc-TPP1** forms the black dots. After coincubating

https://doi.org/10.1021/acs.nanolett.2c02612
Nano Lett. 2022, 22, 7588−7596

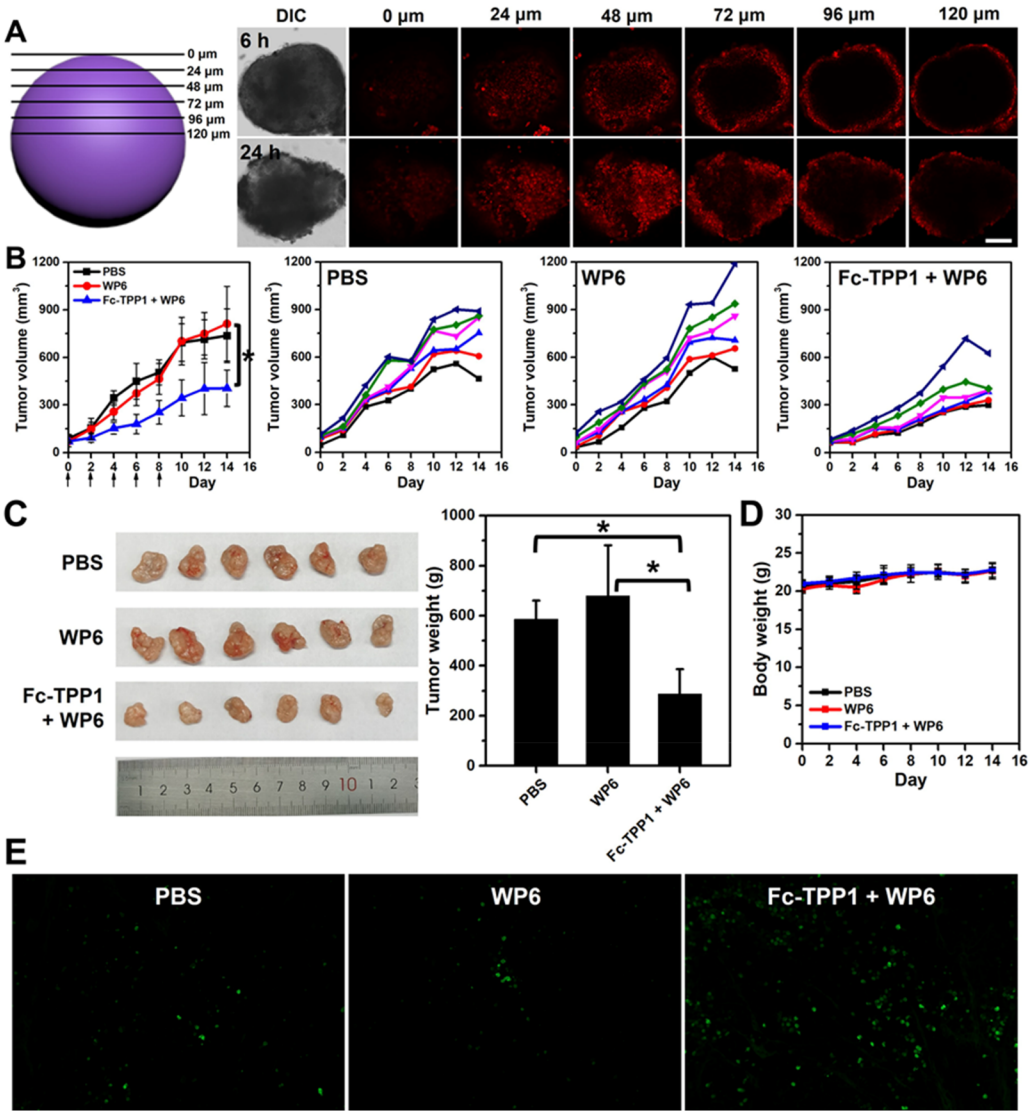

Figure 5. *In vitro* tumor penetration in the Saos-2 MTSs and *in vivo* antitumor efficacy in mice bearing subcutaneous HeLa tumors. (A) The Saos-2 MTSs are cultured with the host−guest complex (**Fc-TPP1**: 50 μM, **WP6**: 50 μM) for 24 h. The MTSs are visualized after 6 and 24 h incubation using CLSM in Z-stacks with 24 μm intervals. **Fc-Cy5.5** (red), scale bar = 100 μm. (B) Tumor volume of mice as a function of anticancer effect. Black arrows indicate dosing schedules. (C) Optical images of dissected tumors and tumor weight at the end of the treatment. (D) Body weight of mice as a function of time. (E) Histological analysis of tumor tissues with TUNEL assay. Data are depicted as mean ± SD *, $P < 0.05$.

the cells with **Fc-TPP1** for 24 h, we observed that the number of organelles within cells decreased, and the black dots are located at the surrounding edge of mitochondria (Figure 4D), indicating the disruption of mitochondrial membranes. For the cells treated with the host−guest complex, we could find that the mitochondria became shrunken after 0.5 h of coincubation, and the cells are unhealthy. Unlike the cells treated with **Fc-TPP1** for 0.5 h, we could observe large amounts of black dots of assemblies formed by the host−guest complex accumulating at the mitochondria (Figure 4E). After incubating for 24 h, the number of organelles within cells treated with the host−guest complex decreases significantly (Figure 4F). These results suggest that the host−guest complex shows much more efficiency in accumulating at the mitochondria and disrupting the integrity of mitochondria.

High-magnification TEM images at the mitochondria region and fast Fourier transform (FFT) pattern further verified that the black dots at mitochondria are formed by self-assembly of **Fc-TPP1** or the host−guest complex. The results show that the Saos-2 cells without treatment do not have the lattice fringe (Figure 4G), indicating the amorphous nanostructures in these cells. In contrast, we can observe ordered lattice fringes obviously in high-magnification TEM images and the bright symmetric diffraction points in FFT patterns (Figure 4H, 4I) in the **Fc-TPP1** and host−guest complex treated cells (24 h). We next perform the inverse FFT for these two regions and then measure the lattice distance. The lattice spacing is detected as 2.6 Å, attributed to the interplanar crystal spacing (−1 0 2) of Fe_3O_4, indicating the formation of Fe-containing crystals inside cells. These results further demonstrate that the black dots at the mitochondria are the nanostructures formed by **Fc-TPP1**.

Furthermore, we performed X-ray photoelectron spectroscopy (XPS) for different treating groups. The XPS results reveal that the Fe-containing compounds are formed in Saos-2 cells after incubating with the host−guest complex, and the cellular uptake is significantly increased by using the host−guest strategy. For the Saos-2 cells without treatment, we

https://doi.org/10.1021/acs.nanolett.2c02612
Nano Lett. 2022, 22, 7588−7596

hardly observe any peaks in the 740−700 eV (Figure 4J), indicating that the cells only contain a bit of Fe-containing compounds. For the cells treated with **Fc-TPP1** for 24 h, the peaks are steady (Figure 4K), and we could hardly fit the peaks corresponding to FeO and Fe, respectively. The calculated content of Fe is 0.04%, which is out of the detection limit of XPS. The peaks for the cells treated with host−guest complex (24 h) are sharper than in the other two groups. After fitting by the nonlinear least-square method (NLS), we find that the peaks consist of FeO and Fe with a content of 69.2% and 30.8%, respectively. The total content of Fe is 0.13% (Figure 4L), which is larger than the cells without and with treatment of **Fc-TPP1**.

The penetration ability and cytotoxicity of **Fc-TPP1** and the host−guest complex are further evaluated in the Saos-2 multicellular tumor spheroids (MTSs) (Figure 5A and Figure S31). After 24 h of incubation, the spherical MTSs collapsed at the periphery with an irregular and shrunken size. The fluorescence of assemblies increased with time elapsed. Compared with the MTSs treated with **Fc-TPP1**, the host−guest complex shows enhanced penetration ability.

We further evaluated the antitumor activity on tumor-bearing mice. The Saos-2 cell line is not used in this experiment considering its nontumorigenicity. Compared with the PBS and **WP6** groups, the host−guest complex treatments slow the tumor growth rates (Figure 5B), and the host−guest complex has a tumor inhibition rate (IR) of 50.9% ($P < 0.05$) at the experiment's end (Figure 5C). The body weight of all mice remained nearly unchanged throughout the experimental period, and all mice did not show noticeable signs of toxicity and abnormal behaviors during the treatment (Figure 5D). Hematoxylin and eosin (H&E) staining showed that the tumors treated with the host−guest complex had less densely packed cells and extensive nuclear shrinkage and cavum compared to those treated with PBS (Figure S32). Notably, the tumors treated with the host−guest complex contained many apoptotic cells (green fluorescence, Figure 5E). These results suggest that the host−guest complex in this work could penetrate into the MTSs, inhibit tumor growth, and induce cell apoptosis signal pathways, resulting in cancer cell death *in vitro* and in the tumor-bearing mice model.

In summary, this work reports utilizing the host−guest complexation to modulate the enzymatic kinetics of peptidic assemblies for cancer therapy. The results showed that introducing host−guest complexation in the enzyme-instructed self-assembly of peptides could enhance the cellar uptake of peptide assemblies and control the final bioactivity of peptides in cancer cells. Our results also suggested that the accumulation of peptide assemblies in the mitochondria could induce the ferroptosis of cancer cells, which could further disrupt the mitochondria and induce apoptosis of cancer cells. This study provided a new and general strategy to kinetically control enzymatic assemblies in living cells, which offered a new avenue for targeted cancer therapy.

■ ASSOCIATED CONTENT

Supporting Information

The Supporting Information is available free of charge at https://pubs.acs.org/doi/10.1021/acs.nanolett.2c02612.

Experimental materials and instruments, experimental methods, characterizations, and supplemental Figures S1−S32; NMR and MS spectra for all compounds. (PDF)

■ AUTHOR INFORMATION

Corresponding Author

Huaimin Wang − *Key Laboratory of Precise Synthesis of Functional Molecules of Zhejiang Province, School of Science, Department of Chemistry, Westlake University; Institute of Natural Sciences, Westlake Institute for Advanced Study, Hangzhou 310024 Zhejiang Province, China;* orcid.org/0000-0002-8796-0367; Email: wanghuaimin@westlake.edu.cn

Authors

Xuejiao Yang − *Key Laboratory of Precise Synthesis of Functional Molecules of Zhejiang Province, School of Science, Department of Chemistry, Westlake University; Institute of Natural Sciences, Westlake Institute for Advanced Study, Hangzhou 310024 Zhejiang Province, China*

Bihan Wu − *Department of Chemistry, Zhejiang University, Hangzhou 310027, P. R. China; Key Laboratory of Precise Synthesis of Functional Molecules of Zhejiang Province, School of Science, Department of Chemistry, Westlake University; Institute of Natural Sciences, Westlake Institute for Advanced Study, Hangzhou 310024 Zhejiang Province, China*

Jiong Zhou − *State Key Laboratory of Chemical Engineering, Key Laboratory of Excited-State Materials of Zhejiang Province, Stoddart Institute of Molecular Science, Department of Chemistry, Zhejiang University, Hangzhou 310027, P. R. China;* orcid.org/0000-0002-3916-0189

Honglei Lu − *Key Laboratory of Precise Synthesis of Functional Molecules of Zhejiang Province, School of Science, Department of Chemistry, Westlake University; Institute of Natural Sciences, Westlake Institute for Advanced Study, Hangzhou 310024 Zhejiang Province, China*

Hongyue Zhang − *Key Laboratory of Precise Synthesis of Functional Molecules of Zhejiang Province, School of Science, Department of Chemistry, Westlake University; Institute of Natural Sciences, Westlake Institute for Advanced Study, Hangzhou 310024 Zhejiang Province, China*

Feihe Huang − *State Key Laboratory of Chemical Engineering, Key Laboratory of Excited-State Materials of Zhejiang Province, Stoddart Institute of Molecular Science, Department of Chemistry, Zhejiang University, Hangzhou 310027, P. R. China; ZJU-Hangzhou Global Scientific and Technological Innovation Center, Hangzhou 311215, P. R. China; Green Catalysis Center and College of Chemistry, Zhengzhou University, Zhengzhou 450001, P. R. China;* orcid.org/0000-0003-3177-6744

Complete contact information is available at: https://pubs.acs.org/10.1021/acs.nanolett.2c02612

Author Contributions

#X.Y. and B.W. contributed equally.

Notes

The authors declare no competing financial interest.

■ ACKNOWLEDGMENTS

This project was supported by the National Natural Science Foundation of China (82022038), Westlake Education Foundation. We thank the Instrumentation and Service Center

for Molecular Sciences, Instrumentation and Service Center for Physical Sciences, and Biomedical Research Core Facilities at Westlake University for the assistance with measurements. F.H.H. thanks the National Natural Science Foundation of China (22035006) and Zhejiang Provincial Natural Science Foundation of China (LD21B020001) for financial support.

REFERENCES

(1) Whitesides, G. M.; Grzybowski, B. Self-assembly at all scales. *Science* **2002**, *295* (5564), 2418−2421.
(2) He, H.; Tan, W.; Guo, J.; Yi, M.; Shy, A. N.; Xu, B. Enzymatic Noncovalent Synthesis. *Chem. Rev.* **2020**, *120* (18), 9994−10078.
(3) Wu, H.; Fuxreiter, M. The structure and dynamics of higher-order assemblies: amyloids, signalosomes, and granules. *Cell* **2016**, *165* (5), 1055−1066.
(4) Yang, Z.; Xu, K.; Guo, Z.; Guo, Z.; Xu, B. Intracellular enzymatic formation of nanofibers results in hydrogelation and regulated cell death. *Adv. Mater.* **2007**, *19* (20), 3152−3156.
(5) Cheng, K.; Ding, Y.; Zhao, Y.; Ye, S.; Zhao, X.; Zhang, Y.; Ji, T.; Wu, H.; Wang, B.; Anderson, G. J.; Ren, L.; Nie, G. Sequentially Responsive Therapeutic Peptide Assembling Nanoparticles for Dual-Targeted Cancer Immunotherapy. *Nano Lett.* **2018**, *18* (5), 3250−3258.
(6) Yang, X.; Cao, Z.; Lu, H.; Wang, H. In Situ Construction of Functional Assemblies in Living Cells for Cancer Therapy. *Adv. Healthcare Mater.* **2021**, *10* (14), e2100381.
(7) Liang, G. L.; Ren, H. J.; Rao, J. H. A biocompatible condensation reaction for controlled assembly of nanostructures in living cells. *Nat. Chem.* **2010**, *2* (1), 54−60.
(8) Jeena, M. T.; Palanikumar, L.; Go, E. M.; Kim, I.; Kang, M. G.; Lee, S.; Park, S.; Choi, H.; Kim, C.; Jin, S. M.; Bae, S. C.; Rhee, H. W.; Lee, E.; Kwak, S. K.; Ryu, J. H. Mitochondria localization induced self-assembly of peptide amphiphiles for cellular dysfunction. *Nat. Commun.* **2017**, *8* (1), 26.
(9) Shi, J. F.; Schneider, J. P. De novo Design of Selective Membrane-Active Peptides by Enzymatic Control of Their Conformational Bias on the Cell Surface. *Angew. Chem., Int. Ed.* **2019**, *58* (39), 13706−13710.
(10) Pires, R. A.; Abul-Haija, Y. M.; Costa, D. S.; Novoa-Carballal, R.; Reis, R. L.; Ulijn, R. V.; Pashkuleva, I. Controlling Cancer Cell Fate Using Localized Biocatalytic Self-Assembly of an Aromatic Carbohydrate Amphiphile. *J. Am. Chem. Soc.* **2015**, *137* (2), 576−579.
(11) Tanaka, A.; Fukuoka, Y.; Morimoto, Y.; Honjo, T.; Koda, D.; Goto, M.; Maruyama, T. Cancer Cell Death Induced by the Intracellular Self-Assembly of an Enzyme-Responsive Supramolecular Gelator. *J. Am. Chem. Soc.* **2015**, *137* (2), 770−775.
(12) Versluis, F.; van Elsland, D. M.; Mytnyk, S.; Perrier, D. L.; Trausel, F.; Poolman, J. M.; Maity, C.; le Sage, V. A. A.; van Kasteren, S. I.; van Esch, J. H.; Eelkema, R. Negatively Charged Lipid Membranes Catalyze Supramolecular Hydrogel Formation. *J. Am. Chem. Soc.* **2016**, *138* (28), 8670−8673.
(13) Cai, Y. B.; Shen, H. S.; Zhan, J.; Lin, M. L.; Dai, L. H.; Ren, C. H.; Shi, Y.; Liu, J. F.; Gao, J.; Yang, Z. M. Supramolecular "Trojan Horse" for Nuclear Delivery of Dual Anticancer Drugs. *J. Am. Chem. Soc.* **2017**, *139* (8), 2876−2879.
(14) Li, J.; Shi, K.; Sabet, Z. F.; Fu, W.; Zhou, H.; Xu, S.; Liu, T.; You, M.; Cao, M.; Xu, M. New power of self-assembling carbonic anhydrase inhibitor: Short peptide-constructed nanofibers inspire hypoxic cancer therapy. *Sci. Adv.* **2019**, *5* (9), eaax0937.
(15) Zhang, M. M.; Guan, Y.; Dang, Z.; Zhang, P. G.; Zheng, Z.; Chen, L.; Kuang, W.; Wang, C. C.; Liang, G. L. Directly observing intracellular nanoparticle formation with nanocomputed tomography. *Sci. Adv.* **2020**, *6* (43), eaba3190.
(16) Pieszka, M.; Han, S.; Volkmann, C.; Graf, R.; Lieberwirth, I.; Landfester, K.; Ng, D. Y.; Weil, T. Controlled Supramolecular Assembly Inside Living Cells by Sequential Multistaged Chemical Reactions. *J. Am. Chem. Soc.* **2020**, *142* (37), 15780−15789.
(17) Wang, J.; Hu, L.; Zhang, H.; Fang, Y.; Wang, T.; Wang, H. Intracellular Condensates of Oligopeptide for Targeting Lysosome and Addressing Multiple Drug Resistance of Cancer. *Adv. Mater.* **2022**, *34* (1), 2104704.
(18) Wang, H.; Feng, Z.; Xu, B. Assemblies of Peptides in a Complex Environment and their Applications. *Angew. Chem., Int. Ed.* **2019**, *58* (31), 10423−10432.
(19) Feng, Z.; Wang, H.; Xu, B. Instructed Assembly of Peptides for Intracellular Enzyme Sequestration. *J. Am. Chem. Soc.* **2018**, *140* (48), 16433−16437.
(20) Feng, Z.; Wang, H.; Wang, S.; Zhang, Q.; Zhang, X.; Rodal, A. A.; Xu, B. Enzymatic Assemblies Disrupt the Membrane and Target Endoplasmic Reticulum for Selective Cancer Cell Death. *J. Am. Chem. Soc.* **2018**, *140* (30), 9566−9573.
(21) Feng, Z.; Wang, H.; Zhou, R.; Li, J.; Xu, B. Enzyme-Instructed Assembly and Disassembly Processes for Targeting Downregulation in Cancer Cells. *J. Am. Chem. Soc.* **2017**, *139* (11), 3950−3953.
(22) Yang, X.; Lu, H.; Tao, Y.; Zhou, L.; Wang, H. Spatiotemporal Control over Chemical Assembly in Living Cells by Integration of Acid-Catalyzed Hydrolysis and Enzymatic Reactions. *Angew. Chem., Int. Ed.* **2021**, *60* (44), 23797−23804.
(23) Hirst, A. R.; Roy, S.; Arora, M.; Das, A. K.; Hodson, N.; Murray, P.; Marshall, S.; Javid, N.; Sefcik, J.; Boekhoven, J.; van Esch, J. H.; Santabarbara, S.; Hunt, N. T.; Ulijn, R. V. Biocatalytic induction of supramolecular order. *Nat. Chem.* **2010**, *2* (12), 1089−1094.
(24) Wang, H. M.; Feng, Z. Q. Q.; Xu, B. Instructed Assembly as Context-Dependent Signaling for the Death and Morphogenesis of Cells. *Angew. Chem., Int. Ed.* **2019**, *58* (17), 5567−5571.
(25) Gu, H.; Mu, S.; Qiu, G.; Liu, X.; Zhang, L.; Yuan, Y.; Astruc, D. Redox-stimuli-responsive drug delivery systems with supramolecular ferrocenyl-containing polymers for controlled release. *Coord. Chem. Rev.* **2018**, *364*, 51−85.
(26) Zhou, J.; Yu, G.; Huang, F. Supramolecular chemotherapy based on host−guest molecular recognition: a novel strategy in the battle against cancer with a bright future. *Chem. Soc. Rev.* **2017**, *46* (22), 7021−7053.
(27) Yu, G.; Jie, K.; Huang, F. Supramolecular amphiphiles based on host−guest molecular recognition motifs. *Chem. Rev.* **2015**, *115* (15), 7240−7303.
(28) Yu, G.; Xue, M.; Zhang, Z.; Li, J.; Han, C.; Huang, F. A water-soluble pillar[6]arene: synthesis, host-guest chemistry, and its application in dispersion of multiwalled carbon nanotubes in water. *J. Am. Chem. Soc.* **2012**, *134* (32), 13248−13251.
(29) Hu, L.; Li, Y.; Lin, X.; Huo, Y.; Zhang, H.; Wang, H. Structure-Based Programming of Supramolecular Assemblies in Living Cells for Selective Cancer Cell Inhibition. *Angew. Chem., Int. Ed.* **2021**, *60* (40), 21807−21816.
(30) Pires, R. A.; Abul-Haija, Y. M.; Costa, D. S.; Novoa-Carballal, R.; Reis, R. L.; Ulijn, R. V.; Pashkuleva, I. Controlling cancer cell fate using localized biocatalytic self-assembly of an aromatic carbohydrate amphiphile. *J. Am. Chem. Soc.* **2015**, *137* (2), 576−9.
(31) Ni, M.; Zhang, N.; Xia, W.; Wu, X.; Yao, C.; Liu, X.; Hu, X.-Y.; Lin, C.; Wang, L. Dramatically Promoted Swelling of a Hydrogel by Pillar[6]arene−Ferrocene Complexation with Multistimuli Responsiveness. *J. Am. Chem. Soc.* **2016**, *138* (20), 6643−6649.
(32) Zhou, J.; Du, X.; Yamagata, N.; Xu, B. Enzyme-Instructed Self-Assembly of Small D-Peptides as a Multiple-Step Process for Selectively Killing Cancer Cells. *J. Am. Chem. Soc.* **2016**, *138* (11), 3813−23.
(33) Burns, R. J.; Smith, R. A.; Murphy, M. P. Synthesis and characterization of thiobutyltriphenylphosphonium bromide, a novel thiol reagent targeted to the mitochondrial matrix. *Arch. Biochem. Biophys.* **1995**, *322* (1), 60−68.
(34) Peng, L.; Feng, A.; Huo, M.; Yuan, J. Ferrocene-based supramolecular structures and their applications in electrochemical responsive systems. *Chem. Commun.* **2014**, *50* (86), 13005−13014.
(35) Duan, Q.; Cao, Y.; Li, Y.; Hu, X.; Xiao, T.; Lin, C.; Pan, Y.; Wang, L. pH-Responsive Supramolecular Vesicles Based on Water-

https://doi.org/10.1021/acs.nanolett.2c02612
Nano Lett. 2022, 22, 7588−7596

Soluble Pillar[6]arene and Ferrocene Derivative for Drug Delivery. *J. Am. Chem. Soc.* **2013**, *135* (28), 10542−10549.
(36) Westermann, B. Mitochondrial fusion and fission in cell life and death. *Nat. Rev. Mol. Cell Biol.* **2010**, *11* (12), 872−884.
(37) Elmore, S. Apoptosis: a review of programmed cell death. *Toxicol. Pathol.* **2007**, *35* (4), 495−516.
(38) Cao, J. Y.; Dixon, S. J. Mechanisms of ferroptosis. *Cell. Mol. Life Sci.* **2016**, *73* (11−12), 2195−209.
(39) Dixon, S. J.; Lemberg, K. M.; Lamprecht, M. R.; Skouta, R.; Zaitsev, E. M.; Gleason, C. E.; Patel, D. N.; Bauer, A. J.; Cantley, A. M.; Yang, W. S.; Morrison, B., 3rd; Stockwell, B. R. Ferroptosis: an iron-dependent form of nonapoptotic cell death. *Cell* **2012**, *149* (5), 1060−72.
(40) Chen, C.; Wang, D.; Yu, Y.; Zhao, T.; Min, N.; Wu, Y.; Kang, L.; Zhao, Y.; Du, L.; Zhang, M.; Gong, J.; Zhang, Z.; Zhang, Y.; Mi, X.; Yue, S.; Tan, X. Legumain promotes tubular ferroptosis by facilitating chaperone-mediated autophagy of GPX4 in AKI. *Cell Death Dis.* **2021**, *12* (1), 65.
(41) Gao, M.; Yi, J.; Zhu, J.; Minikes, A. M.; Monian, P.; Thompson, C. B.; Jiang, X. Role of Mitochondria in Ferroptosis. *Mol. Cell* **2019**, *73* (2), 354−363.e3.
(42) Bock, F. J.; Tait, S. W. G. Mitochondria as multifaceted regulators of cell death. *Nat. Rev. Mol. Cell. Biol.* **2020**, *21* (2), 85−100.
(43) Basit, F.; van Oppen, L. M.; Schockel, L.; Bossenbroek, H. M.; van Emst-de Vries, S. E.; Hermeling, J. C.; Grefte, S.; Kopitz, C.; Heroult, M.; Hgm Willems, P.; Koopman, W. J. Mitochondrial complex I inhibition triggers a mitophagy-dependent ROS increase leading to necroptosis and ferroptosis in melanoma cells. *Cell Death Dis.* **2017**, *8* (3), e2716.

https://doi.org/10.1021/acs.nanolett.2c02612
Nano Lett. 2022, 22, 7588−7596